Dimer desorption from solid argon films electronically excited by MeV He ions

C. T. Reimann*
Naval Research Laboratory, Washington, D.C. 20375

W. L. Brown
AT&T Bell Laboratories, Murray Hill, New Jersey 07901

D. E. Grosjean and M. J. Nowakowski†
Department of Nuclear Engineering and Engineering Physics, University of Virginia, Charlottesville, Virginia 22901
and AT&T Bell Laboratories, Murray Hill, New Jersey 07901

(Received 15 April 1991; revised manuscript received 26 August 1991)

Electronic excitation of solid Ar films by MeV He^+ ions gives rise to broad luminescence bands centered at 1110 and 1265 Å. We have examined the spatial and temporal characteristics of these dimer luminescence bands. Observing *all* the luminescence, we measure a spectrum that is dominated by the 1265-Å band. This band is from decay of vibrationally relaxed $Ar_2^*(^{1,3}\Sigma_u^+)$ trapped in the bulk of the Ar film. Observing only the luminescence from a plume of desorbed particles *in front* of the excited Ar film, we observe a long-lived 1110-Å luminescence band with a long-wavelength tail extending down to the region around 1265 Å. This band is from decay of gas-phase $Ar_2^*(^3\Sigma_u^+;1_u,0_u^-)$ in various degrees of vibrational relaxation. The Ar_2^* ejection kinetic energy (KE), as well as the degree of vibrational relaxation, are important clues to the mechanisms of dimer formation and desorption. We observe a delayed onset of the luminescence under pulsed excitation if the base of the luminescent plume is hidden from view. The average delayed onset time is a time of flight, the value of which indicates that the average KE of the desorbed Ar_2^* is 0.1 eV but ranges as low as 0.06 eV for dimers in highly vibrationally excited states. The temporal width of the delayed onset is consistent with a hemispherical plume shape. We have fitted the observed 1110-Å luminescence band with a linear combination of quantum mechanically calculated luminescence spectra of the vibrational levels of $Ar_2^*(^3\Sigma_u^+;1_u,0_u^-)$. The resulting vibrational-state distribution is non-Boltzmann and increases sharply with decreasing vibrational quantum number, indicating a considerable degree of vibrational relaxation. These results are discussed in terms of simple models of the Ar_2^*-desorption process. We hypothesize that Ar_2^* is ejected with a KE around 0.1 eV after dissociative recombination of an electron with a near-surface self-trapped hole, Ar_2^+, and subsequent dimerization of the energetic Ar^*. Many-body collisions occurring during dimerization effectively relax the vibrational state of the dimer.

I. INTRODUCTION

When solid argon is electronically stimulated by ions, electrons, or photons, substantial lattice rearrangements occur as the electronic energy relaxes prior to radiative decay.[1] Particle desorption and luminescence are two diagnostics of the concomitant lattice dynamics. Under 1.5-MeV He^+-ion excitation, a net desorption yield of about 40 atoms per incident ion has been measured.[2–6] The ejection yield has been assumed to consist mostly of ground-state atoms,[2–9] but ejected excited-state atoms,[10–12] excited-state dimers,[6,13–16] and ions[10,11] have also been observed. Desorption is a direct consequence of the conversion of some fraction of electronically deposited potential energy into kinetic energy (KE) during lattice relaxation.

Electronically excited argon films also emit copious amounts of luminescence in the vacuum ultraviolet (vuv).[17] Dramatic lattice relaxation effects are seen in the luminescence spectrum, features of which are strongly red shifted relative to the excitonic levels of unperturbed solid argon.[17] As shown in detail below, two broad molecular-type luminescence bands are observed at 1110 Å (*W* band) and 1265 Å (*M* band). The 1110-Å band is from radiative decay of vibrationally excited Ar_2^*, whereas the 1265-Å band is from radiative decay of vibrationally relaxed Ar_2^*.[17] These dimers exist with internuclear separations that are considerably smaller than the interatomic spacing in the undisturbed Ar lattice. Earlier work has focused on delineating the correlation between the luminescence and desorption phenomena and has speculated about possible desorption mechanisms.[5,6,13]

The dynamics of Ar_2^* formation, relaxation, and decay can be followed by observing the two molecular luminescence bands centered at 1110 and 1265 Å. An analysis of the film thickness dependences of the luminescence features indicates that 1265-Å luminescence comes dominantly from Ar_2^* trapped in the bulk of the Ar film[6,18] while 1110-Å luminescence could come from both surface-trapped[1,18,19] Ar_2^* and desorbed[6,13–16] Ar_2^*. Schematics of these situations are shown in Figs. 1(a)–1(d). The observation of luminescence emitted from

in front of the film indicates that at least *some* of the 1110-Å luminescence arises from a plume of desorbed[6,14–16] Ar_2^*. However, due to geometrical constraints in the experimental setup described in Ref. 6, it is not known what fraction of the total 1110-Å luminescence comes from the plume. Also, although the Ar_2^* ejection KE has been estimated to be around 0.1 eV,[14,20] a reliable value for this KE has not yet been determined. Such a determination would assist in understanding the operative Ar_2^*-ejection mechanisms. Consequently, an improved experimental examination of the spatial and temporal characteristics of the molecular-type luminescence bands is the motivation for the work described in this paper. Brief summaries of this work have appeared elsewhere.[15,16]

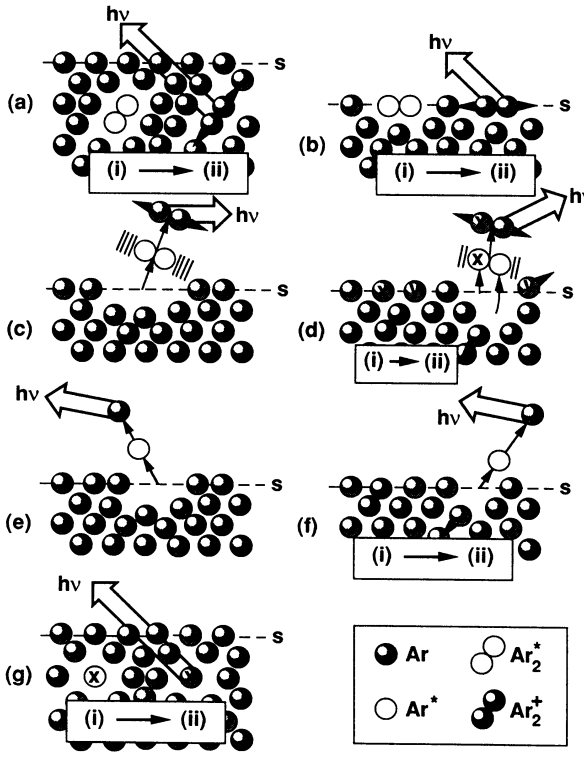

FIG. 1. Schematic of exciton and hole decay processes in solid argon. The steps in a given process proceed from (i) to (ii). (a) Cavity formation around a bulk self-trapped Ar_2^* and subsequent repulsive radiative decay; (b) surface self-trapped Ar_2^* and subsequent repulsive radiative decay; (c) cavity ejection of a vibrationally excited surface self-trapped Ar_2^* and subsequent radiative decay of the Ar_2^* in space; (d) repulsive recombination of an electron with Ar_2^+ and subsequent ejection of vibrationally excited Ar_2^* (electron not shown). The energized atom moving towards the surface has dimerized with the atom labeled "*x*." During dimerization, vibrational relaxation occurs through a collision with atom "*y*" and some other nearby surface atoms. Radiative decay occurs in space; (e) cavity ejection of a surface self-trapped Ar* and eventual radiative decay in space; (f) repulsive recombination of an electron with Ar_2^+ and subsequent ejection of Ar* (electron not shown) and eventual radiative decay in space; (g) cavity formation around a bulk self-trapped Ar* and subsequent radiative decay.

In the present work, a time-of-flight (TOF) technique is employed to determine the KE of desorbed triplet-state dimers $Ar_2^*(^3\Sigma_u^+;1_u,0_u^-)$, which emit luminescence in the 1110-Å band. The average KE of the ejected triplet-state dimers is about 0.10 eV. Ar_2^* emitting luminescence at shorter wavelengths in the 1110-Å band appear to have a lower average KE, 0.06 eV. A spread in KE due to the existence of a velocity distribution, and the angular distribution of dimer desorption, are not unambiguously determined by the modeling discussed below. However, the data are consistent with KE ranging up to 0.3 eV and with dimers being ejected into a hemispherical plume.

The luminescence band of the triplet-state dimers is very broad, indicating that these dimers are created in a wide range of degree of vibrational relaxation. To take advantage of degree of vibrational relaxation as a diagnostic of the dimer ejection mechanism, simulations have been performed of the luminescence spectra of transitions from the vibrational levels of $Ar_2^*(^3\Sigma_u^+;1_u,0_u^-)$ to the ground-state $Ar_2(^1\Sigma_g^+;0_g^+)$. From a fit of a linear combination of these calculated spectra to the observed luminescence spectrum it is seen that the $Ar_2^*(^3\Sigma_u^+;1_u,0_u^-)$ are substantially relaxed vibrationally, though they are not completely so. Linking the deduced vibrational-state distribution to the $Ar_2^*(^3\Sigma_u^+;1_u,0_u^-)$ desorption process still requires the assumption that these species are desorbed directly from the surface rather than being the result of cascading from more highly excited desorbed argon dimers.

The degree of vibrational relaxation as well as the ejection KE of the desorbed dimers serve as key features that distinguish between the applicability of hypothesized Ar_2^*-ejection models. The results from the present experiments are discussed in terms of two distinct Ar_2^*-ejection mechanisms: cavity ejection[6,10,13,20] and repulsive recombination.[6,21] The ejection of a dimer from a cavity is shown schematically in Fig. 1(c). In this ejection mechanism, the lattice around a dimer distorts in order to accommodate the Rydberg electron of the dimer. At the surface, lattice strain can be minimized if the dimer is ejected. Classically dynamics simulations of the cavity ejection of a dimer formed at the surface predict a very low KE for ejected Ar_2^*, typically <0.04 eV,[20] as well as a high degree of vibrational excitation, both in contrast to what is observed.

In situations involving copious electron-hole pair production, such as occur under MeV ion excitation, the repulsive recombination model for dimer ejection[6] may be dominant. An example of this ejection mechanism, shown schematically in Fig. 1(d), occurs via internuclear potential surfaces sketched in Fig. 2. Energetic ejection of Ar_2^* occurs after repulsive recombination of an electron with Ar_2^+ near the surface (process 2 in Fig. 2) and dimerization of a resulting Ar* which happens to be moving towards the surface [Fig. 1(d)]. The translational KE release in process 2 is expected to be of the order of 0.1–0.5 eV, and at the same time, it is intuitively expected that a large degree of vibrational relaxation would result as internal energy is removed from the Ar_2^* during many-body collisions occurring during ejection. The ob-

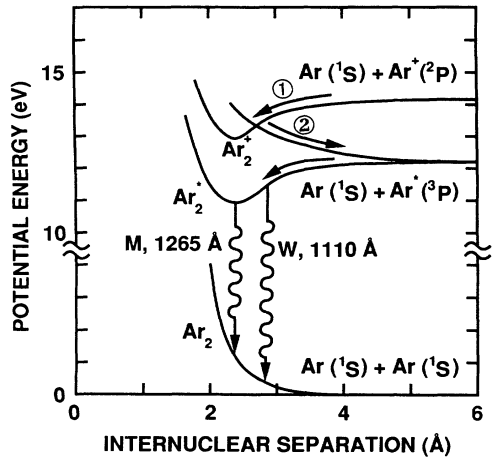

FIG. 2. Internuclear potential-energy surfaces relevant to the ejection processes of electronically stimulated solid argon. In process 1, a hole Ar^+ self-traps to form an ionic dimer, Ar_2^+. In process 2, an electron recombines with Ar_2^+ and a ground-state atom Ar and an excited-state atom Ar* rapidly recede from one another.

servations are consistent with these expectations and with the preliminary results of molecular dynamics calculations designed to simulate the repulsive recombination desorption mechanism.[16,22]

II. EXPERIMENT

Experiments are performed in an ultrahigh vacuum (UHV) chamber with a base pressure of 1×10^{-9} Torr. Ar films are grown on a polished Cu target located near the center of the chamber. To produce an Ar film, the cooled (12 K) target is positioned directly in front of a microchannelplate (MCP) nozzle through which a known quantity of Ar gas is admitted. The resulting films are grown in about 1 min and are typically 2000 Å thick, as measured by Rutherford backscattering (RBS) of 1.5-MeV He^+ ions. Rapid growth at a temperature and pressure below the triplet point causes the films to have a high density of vacancies, dislocations, and stacking faults.[23,24] However, the brief film-growth time ensures that codeposition of impurities is negligible.[6]

To examine luminescence from ion-excited Ar films, a 0.2-m vuv monochromator with an aberration-corrected concave holographic $MgFl_2$-coated Al grating and a channeltron detector is employed. The monochromator has $f/4.5$ collection optics and accepts photons from a broad field of view consisting of a 30-mm region in front of and including the target. Luminescence emitted at around 135° with respect to the direction of the incident ions is monitored. The target translates and rotates in the plane defined by the ion beam and the monochromator input axis. During ion bombardment, the target is positioned so that its rotation axis corresponds to the center of its face and to the center of the ion impact region.

The spatial profile of luminescence from the plume of desorbed material is measured using the experimental setup shown in Fig. 3. The intensities of the various spectral features are monitored as the target is rotated by increasing θ. In the grazing configuration shown, the target edge blocks first bulk and surface luminescence and then successively greater amounts of plume luminescence. In particular, the luminescence spectrum due only to long-lived desorbed $Ar_2^*(^3\Sigma_u^+;1_u,0_u^-)$ can be measured. During these measurements, the target is typically rotated by an angle less than 4° away from the orientation for which the monochromator input axis grazes the target plane. For the 2-cm width of the rotatable block, this corresponds to probing the plume over a range of about 1 mm with a spatial resolution of about 50 μm.

By narrowing the field of view of the monochromator and translating the target instead of rotating it, the spatial structure of the luminescent plume is probed more coarsely, but over an extended 10-mm range.[6] The field of view of the monochromator is limited by mounting a snout with a narrow split over the monochromator input. The resulting spatial resolution is about 1.1 mm.[6] During the measurement, the target is oriented so that the monochromator input axis is parallel to the target surface.

The temporal characteristics of the luminescence are monitored using pulsed 1.5-MeV He^+-ion excitation and the experimental arrangement shown in Fig. 4. A focused ion beam is swept at 126.6 kHz across a small aperture upstream from the target, generating ion pulses as short as 50 nsec. The function generator which triggers the ion beam pulser also triggers a time-to-amplitude converter (TAC). The TAC is stopped by a pulse from the monochromator channeltron and processing electronics. The TAC output pulses are accumulated with a multichannel analyzer (MCA) and the luminescence time decays are transferred to a Digital Equipment Corporation VAX mainframe computer for detailed analysis. The system time resolution is estimated by monitoring the decay of resonance fluorescence at 1067 Å due to desorbed excited $Ar^*(^3P_1)$ atoms.[13] The observed 50-nsec width of

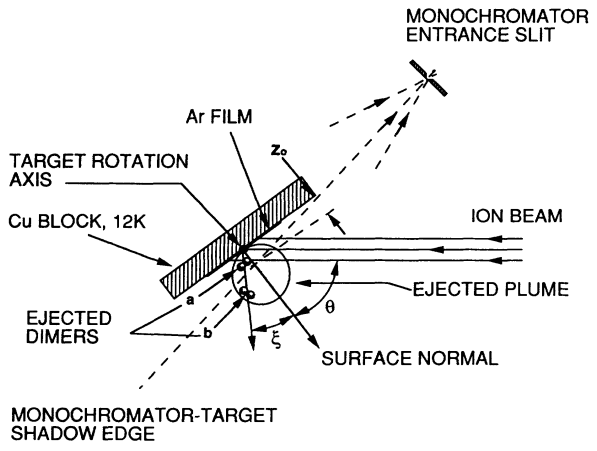

FIG. 3. Geometry for examination of the luminescence plume on a 1-mm spatial scale. Luminescence from dimer *a* cannot reach the monochromator, whereas luminescence from dimer *b* can reach the monochromator.

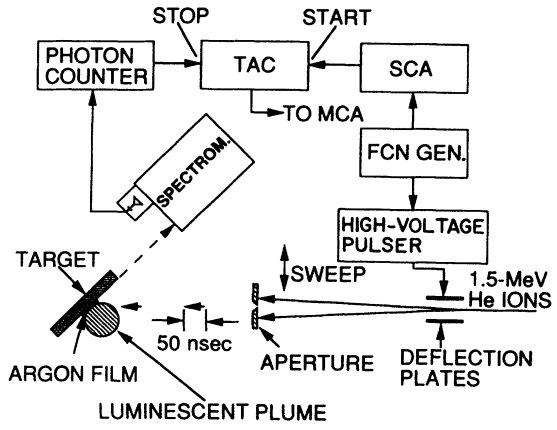

FIG. 4. Electronic setup for time-resolved luminescence decay measurements.

the time decay curve of this fluorescence represents the system time resolution, since the radiative lifetime of the $Ar^*(^3P_1)$ state is less than 10 nsec.[25] The system time resolution is much smaller than the radiative lifetimes of $Ar_2^*(^3\Sigma_u^+;1_u,0_u^-)$, which range from 160 nsec to 3.0 μsec.[26,27] The ion beam is sharply focused at the position of the pulsing aperture, and there is no background signal due to an ion beam "penumbra."

III. RESULTS

A typical luminescence spectrum from 1.5-MeV He^+-ion-excited solid argon in the wavelength range 1000–1400 Å is shown in Fig. 5. In this measurement, the monochromator views luminescence from the bulk of the film as well as from the surface and any desorbed species. Five prominent features were noted: two broad molecular-type luminescence bands labeled M and W; two nearly resolution-limited lines; and a band of intermediate width. The two narrow lines correspond so closely to two atomic resonances of isolated argon atoms, $^1P_1$ and $^3P_1$, that they are assumed to be emitted from desorbed excited Ar*,[13] as shown in Figs. 1(e) and 1(f). The feature slightly to the red of $^3P_1$ is due to radiative decay of an excited Ar* trapped in the argon lattice; this species is an atomic-type self-trapped exciton (ASTE).[17,18] The M and W bands are due to radiative decay of electronically excited dimers $Ar_2^*(^3\Sigma_u^+;1_u,0_u^-)$ and $Ar_2^*(^1\Sigma_u^+;0_u^+)$. The M band is dominantly from the bulk of the excited films[6,18] and comes from completely vibrationally relaxed Ar_2^*, also known as molecular-type self-trapped excitons (MSTE).[1] A schematic of these centers is shown in Fig. 1(a). The W band is associated with the surface of the sample, and arises either from surface-trapped MSTE[19] as shown in Fig. 1(b), or from desorbed[6,13] Ar_2^* as shown in Fig. 1(c) and 1(d). W-band luminescence has been observed to come at least partly[6,14] or even wholly[14–16] from desorbed species.

The dependence of the luminescence spectrum on target angle is shown in Fig. 6. As the target is rotated from a "head-on" configuration in which all luminescence is observed to a more "grazing" one in which the target edge blocks more and more of the luminescence, the relative contributions from the various luminescence

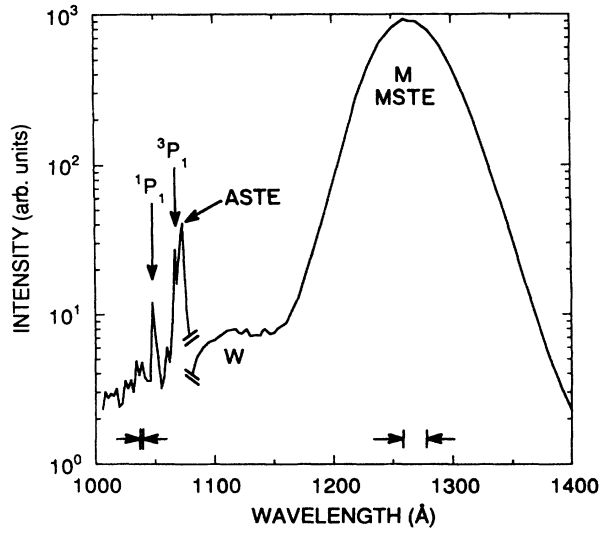

FIG. 5. Luminescence spectrum of solid argon under 1.5-MeV He^+-ion bombardment. Both bulk and plume luminescence are visible to the monochromator. The resolutions employed in different spectral regions are indicated by the horizontal arrows. The observed features are discussed in the text.

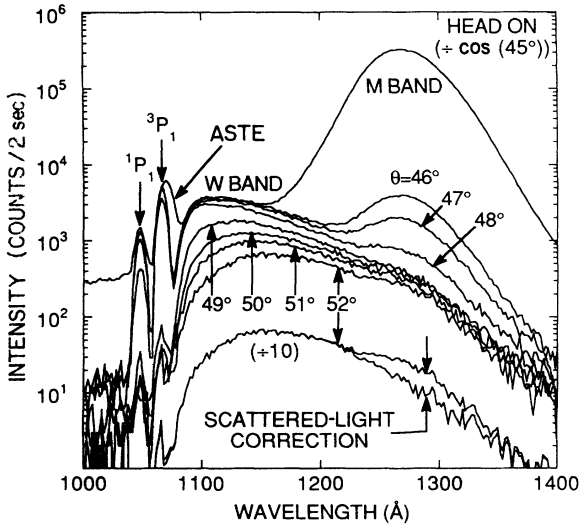

FIG. 6. Variation of the luminescence spectrum as the target is rotated from a head-on configuration in which all luminescence is measured by the monochromator ($\theta < 48°$) to a grazing configuration in which the luminescent plume is gradually occluded ($\theta \geq 49°$). In the "head-on" case, incident ions impact perpendicular to the target surface, whereas in the other cases shown the impact angle is about 45°. In accordance with the model presented in Ref. 6, in which luminescence and desorption yields are proportional to the number of excitations created within a certain distance of the surface, the "head-on" spectrum is divided by cos(45°) so that its intensity may be properly compared with the intensities of the other curves. The scattered M-band light correction to the $\theta = 52°$ data is shown with the curves shifted down for clarity.

features change. Luminescence features arising from luminescence centers in the bulk drop smoothly as the target is rotated from the head-on configuration. The drop of the ASTE (not completely resolved in Fig. 6) and M band can be approximately modeled by considering the refraction of bulk luminescence as it exits the film. Initially, the $^1P_1$ line displays a smooth drop along with the ASTE and M bands. It is therefore hypothesized that there is a second bulk ASTE band which partially overlaps the $^1P_1$ line. The slight asymmetry observed in the $^1P_1$ feature shown in Fig. 5 is also indicative of the existence of this hypothesized ASTE.

The atomic features $^1P_1$ and $^3P_1$ disappear abruptly as the target angle θ (defined in Fig. 3) exceeds 48.5°. The lifetimes of the desorbed excited atoms are 8.4-nsec ($^3P_1$) and 2.0 nsec ($^1P_1$),[25] and even for a desorption KE as high as 1 eV, the light from these emitting atoms would be blocked by turning the edge of the Cu target only 0.1° past the input axis of the monochromator. The dependence of the intensity of the atomic resonance lines on target angle allows a determination of the target angle at which the monochromator input axis grazes the target surface.

As the target angle is moved from the head-on configuration to the grazing configuration, it is seen from Fig. 6 that the intensity of the W band hardly changes, in contrast to the behavior of the M band and ASTE band. As the target rotation is increased further, the W band drops smoothly in intensity. It can be concluded that the W-band luminescence is dominantly due to a plume of desorbed species[6,13–16] rather than to surface-trapped species.[17,19] Figure 6 shows a change in the shape of the W-band spectrum that occurs as the plume is blocked, indicating that the spatial extent of the plume is much smaller at a wavelength of 1100 Å than it is at 1200 Å.

As the bulk luminescence is hidden by rotating the target, a feature centered at 1265 Å remains detectable. The strength of this feature increases with film thickness and thus represents scattered M-band luminescence from the bulk of the Ar film. This feature can be smoothly removed by subtracting a multiple of the M-band spectrum obtained with the target in the head-on orientation. The result of this correction is shown in Fig. 6. It can be seen that the W band possesses a low-energy tail that extends into and past the region occupied by the M band from the bulk. Thus, dimers are desorbed in a full range of degrees of vibrational relaxation.

The target rotation experiments probe the first 1 mm of the plume. Using the differential plume examination geometry outlined above, the plume is delineated on a much broader 10-mm spatial scale. The result is shown in Fig. 7. Beyond the portion of the plume which extends only 1–2 mm out in front of the target, there is a much longer "tail." Under ion excitation, the fraction of the total luminescence signal that can be attributed to the long tail is about 10%. Under synchrotron excitation of solid argon films, this long tail comprises a much greater fraction of the total luminescence signal, approximately 50%.[14] The significance of this long spatial tail is discussed below in terms of a possible contribution to luminescence from the metastable molecular state

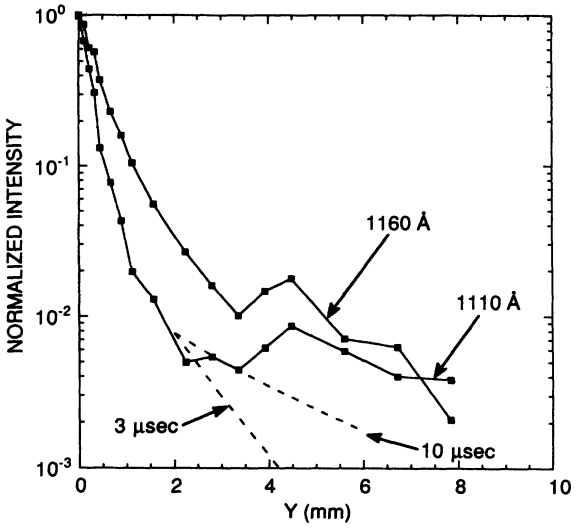

FIG. 7. Spatial profiles of the luminescent plume viewed on a 1-cm scale. The dashed lines are model curves discussed in Sec. VI.

$Ar_2^*(0_u^-)$.

Luminescence decay curves measured at a series of wavelengths in the W and M bands are shown in Fig. 8. The wavelength resolution is 25 Å. In this measurement, the monochromator views luminescence from the bulk of the film as well as from the surface and any desorbed species. Singlet luminescence from $Ar_2^*(^1\Sigma_u^+;0_u^+)$ can be identified by the presence of a resolution-limited prompt feature visible at $t=0$ nsec. The triplet luminescence de-

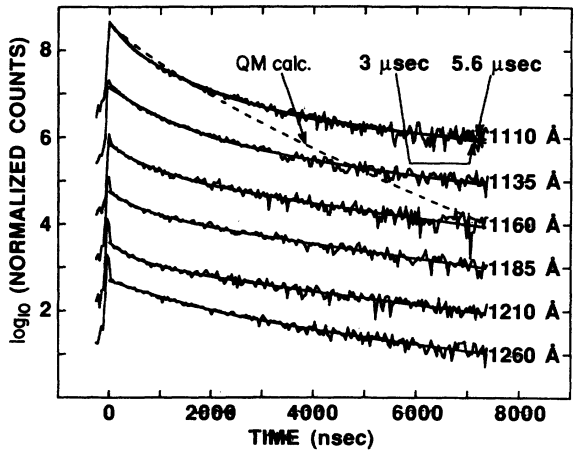

FIG. 8. Luminescence time decays measured at various wavelengths in the W band with the bulk luminescence blocked but the luminescence plume completely visible. The curves are shifted for clarity. The smooth lines are fits to a six-exponential decay as discussed in Sec. IV. For wavelengths of 1135-Å and greater, a tail lifetime (for $t > 5000$ nsec) of 3 μsec is assumed. For a wavelength of 1110 Å, a longer tail lifetime of 5.6 μsec results from the fits. The dashed curve is a simulated luminescence decay based on spectral simulations and is discussed in Sec. VI.

cays from $Ar_2^*(^3\Sigma_u^+;1_u,0_u^-)$ are identified by their μsec decay times. The ratio of the singlet to triplet luminescence signals becomes smaller for shorter wavelengths in the W band. The triplet luminescence decays from $Ar_2^*(^3\Sigma_u^+;1_u,0_u^-)$ are nonexponential. This nonexponentiality results partly from contributions at a given wavelength from several vibrational levels of Ar_2^* with different radiative lifetimes.[17,26,27] Focusing on the early time decay behavior past the initial singlet spike, it can be seen that dimers emitting higher-energy photons are characterized by shorter radiative lifetimes, in general agreement with observations as well as with theoretical calculations (Refs. 26, 27, and references therein). The significance of the long-lifetime tail observed at the shortest wavelengths is discussed below in terms of a contribution from the metastable state $Ar_2^*(0_u^-)$.

The result of monitoring luminescence time decays as a function of target angle is shown in Fig. 9. These data correspond to a wavelength setting of 1185 Å with a resolution of 25 Å, but similar measurements were taken at six other wavelengths throughout the W band and M band. For $\theta > 48°$, the prompt spike at $t=0$ nsec corresponding to luminescence of $Ar_2^*(^1\Sigma_u^+;0_u^+)$ abruptly disappears. The lifetime of $Ar_2^*(^1\Sigma_u^+;0_u^+)$, less than 10 nsec,[19] is so short that radiative decay occurs too near to the surface for us to distinguish between surface-trapped and desorbed dimers in this electronic state. As the base of the plume is increasingly hidden, the triplet luminescence decay curves due to $Ar_2^*(^3\Sigma_u^+;1_u,0_u^-)$ display a delayed onset of up to 2000 nsec as observed for the maximum occlusion angle employed. This delayed onset is the time of flight for ejected dimers to leave the shadow of the edge of the Cu target block and become visible to the monochromator. The rounded nature of the onset primarily reflects the various path lengths ejected dimers can take while exiting from the shadow. Normalization of the data in Fig. 9 is by cumulative incident ion fluence during the acquisition of each time decay, and the close correspondence of the curves at long times confirms that long-lived W-band luminescence is dominantly emitted from desorbed $Ar_2^*(^3\Sigma_u^+;1_u,0_u^-)$. The small, prompt spike and tail seen near $t=0$ nsec for blocked plume geometries is scattered light from the blocked portion of the plume. This signal is easily subtracted.

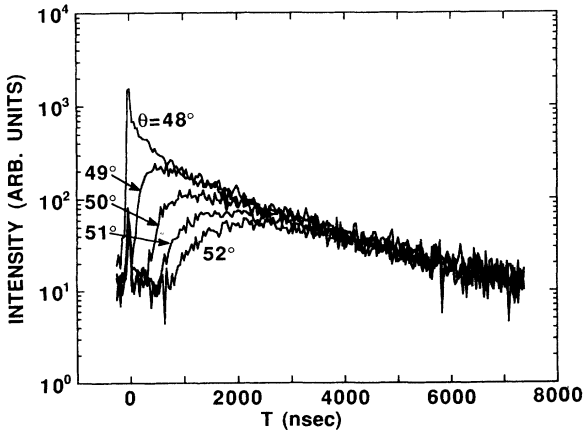

FIG. 9. Luminesecnce time decays measured as the plume is occluded. The delayed onset is related to the time of flight for dimers to escape from the shadow edge of the target and become visible to the monochromator. θ is defined in Fig. 3.

IV. EJECTION KINETIC ENERGY

Luminescence time decays from partially occluded luminescent plumes display delayed and rounded onsets relative to luminescence decays measured while observing the completely unoccluded plume. These delays and rounded onsets are due to variable times of flight of dimers escaping from the shadow of the target edge and becoming visible to the monochromator. These time decays are modeled based on the geometry shown in Fig. 3. Initially, several simplifying assumptions are made. The ion beam is assumed to be narrow with respect to the target width, and the shadow edge is assumed to be parallel to the target face (the angle displayed in Fig. 3 between the target face and the shadow edge is greatly exaggerated). The distance of the shadow edge from the target face is z_0 and depends on the target orientation angle. Ar_2^* is assumed to be desorbed instantaneously at the time of the ion pulse impact. The polar angle distribution of the ejected dimers is taken to be proportional to $\cos^n(\xi)$ where ξ is the polar angle of ejection defined in Fig. 3. (Because the process underlying dimer ejection are electronic in nature, rather than involving direct momentum transfer from the incident ions, the angle of incidence θ of the ion beam does not enter into consideration here.) The dimer velocity is taken to be independent of the azimuthal angle of ejection but may depend on ξ: $v=v_0\cos^m(\xi)$. The ratio $r=(n+1)/(m+1)$ can be treated as a fitting parameter. If $f(t)$ is the luminescence time decay measured while observing the whole plume (i.e., the curves in Fig. 8) and $I(t)$ is the luminescence time decay measured while observing the partially occluded plume (for example, the curves in Fig. 9), then

$$I(t)=f(t)[1-(z_0/v_0t)^r] \tag{4.1}$$

for $t \geq z_0/v_0$ and $I(t)=0$ for $t < z_0/v_0$.

Fits to the simplified model of Eq. (4.1) were performed for time decay data accumulated at a wavelength setting of 1185 Å, a resolution of 25 Å, and a target angle of $\theta=52°$, corresponding to $z_0=0.6$ mm. Two fitting parameters were used: an overall scale factor and the quantity z_0/v_0. $f(t)$ was taken to be a separate fit to the $\theta=48°$ unoccluded plume time decay data using a model consisting of five exponential decays evenly spaced in their rate constants and a separate exponential tail (five parameters total). The $\theta=48°$ time decay and its fit $f(t)$ are shown in Fig. 8, and the delayed onset model fits to the $\theta=52°$ time decay are shown in Fig. 10(a). None of the selections for r results in a good fit, but clearly r cannot be greater than 1. Assuming that the dimer velocity does not depend strongly on ejection angle ξ (i.e., $m=0$), then $r=1$ implies that the plume is hemispherical, with dimers being ejected uniformly in all directions.

The simple model is next embellished. Since the argon film surface is likely to be rough, particularly after the

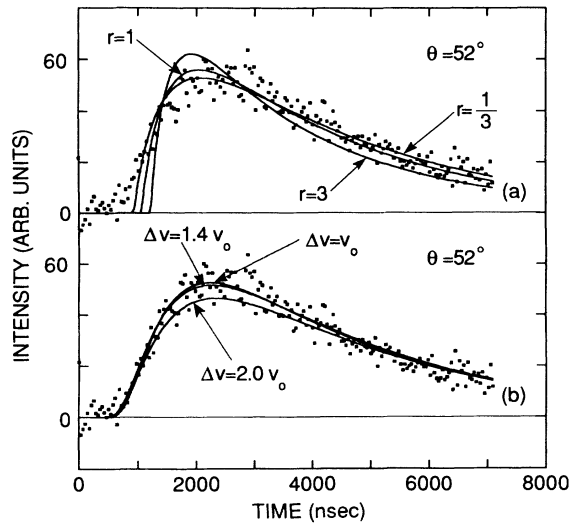

FIG. 10. Model fitting to the luminescence decay measured for a wavelength of 1185 Å and a target angle of $\theta=52°$. (a) Fits to the simple geometrical model of Eq. (4.1). (b) Fits including a velocity distribution with three different assumed velocity FWHM's. For details, see Sec. IV.

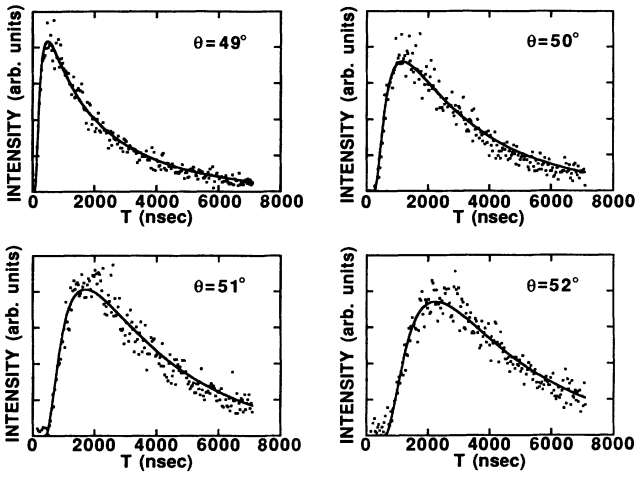

FIG. 11. Panorama of model fits to luminescence decays for a wavelength of 1185 Å and four different target orientations or plume occlusion conditions. $\Delta v=1.4v_0$ was assumed. For details, see Sec. IV.

application of a large fluence of ions,[6] local unit normal vectors will be oriented randomly with respect to the macroscopic surface unit normal vector. Consequently, an ensemble of nonspherical local plumes will average together to form a hemispherical macroscopic plume ($n=0$). A dependence of ejection velocity on local polar angle will, when averaged over the surface roughness, appear to be present as a polar angle independent ($m=0$) *velocity distribution.* Even if the ejection velocity displayed no strong dependence on polar ejection angle, it is reasonable to hypothesize the existence of a velocity distribution for the desorbed Ar_2^*.

To take these modifications into account, $r=1$ is assumed and Eq. (4.1) is convoluted with a simple Gaussian distribution of velocity. A Gaussian distribution is employed both because of its simplicity and because its peak position and its width may be independently varied. Finally, because the plume occlusion shadow made by the target edge is not in general parallel to the target face, as can be seen in Fig. 3, this nonparallelism as well as the finite size of the ion beam impact region are taken into account.

Two parameter fits using the embellished model are performed for different assumed widths of the velocity distribution, and the results are shown for the $\theta=52°$ time decay data in Fig. 10(b). The two parameters are: overall scale and z_0/v_0, where v_0 is the most probable velocity of the velocity distribution. In order to adequately model the rise of the occluded luminescence time decay, rather large fractional velocity widths of the order of 1.0 are needed. A fractional full width at half maximum (FWHM) equal to 1.0 corresponds to a velocity FWHM equal to the most probable velocity in the distribution. For FWHM of the order of 1.0, the quality of the fits as well as the deduced values of the most probable velocity are not very sensitive to the actual assumed value of the FWHM.

For a wavelength setting of 1185 Å, the luminescence decays for occluded plumes are displayed along with delayed luminescence onset model fits in Fig. 11. A fractional velocity FWHM of 1.4 is assumed. The slope of a plot of fitting parameter z_0/v_0 versus target orientation angle θ is inversely proportional to v_0, and hence v_0 and the KE may be calculated. For a wavelength of 1185 Å, the calculated KE is 0.094 eV.

Most probable velocities are obtained from similar fits performed for data taken at six different wavelengths throughout the *W* band. These velocities are converted to KE and are plotted in Fig. 12. A trend in KE is seen, with dimers emitting at lower wavelengths being

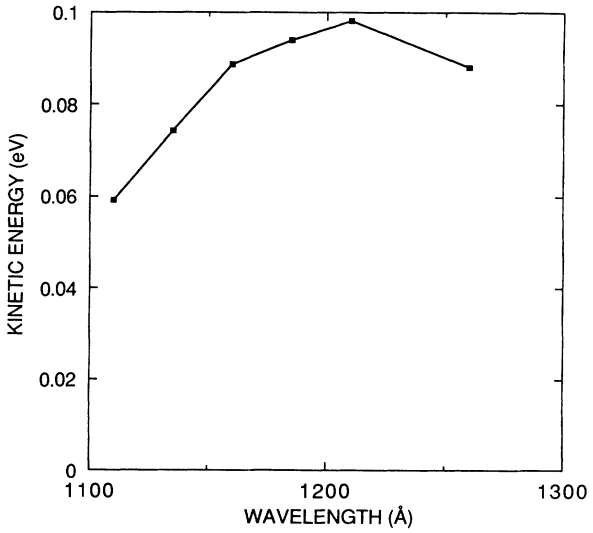

FIG. 12. Kinetic energies resulting from model fitting of luminescence decays measured at various wavelengths in the *W* band. The lines connecting the points are to guide the eye.

desorbed with somewhat lower KE. The typical KE of ejected Ar_2^* ranges from 0.060 to 0.095 eV. If a slightly narrower velocity distribution is assumed, with a fractional FWHM of only 1.0, KE's higher by about 0.01 eV result from the fittings. Including the velocity spread, the highest KE of ejected dimers is around 0.3 eV.

V. DEGREE OF VIBRATIONAL RELAXATION

The ability to measure a luminescence spectrum uniquely associated with desorbed $Ar_2^*(^3\Sigma_u^+;1_u,0_u^-)$ can be exploited to determine the population distribution of the vibrational levels of these desorbed molecules. This distribution and the ejection KE are important clues to the dimer ejection mechanism.

To determine the vibrational distribution, the spectrum $S_{v'}(\lambda)$ from each vibrational level v' of $Ar_2^*(^3\Sigma_u^+;1_u,0_u^-)$ must be calculated, and the observed spectrum of the whole plume must then be fitted to a linear combination of the predicted spectra $S_{v'}(\lambda)$. Using suitable normalization, the fitting coefficients are the relative occupancies of the vibrational levels v' of the ensemble of desorbed dimers.

The simulation of the emission spectrum from vibrational level v' of $Ar_2^*(^3\Sigma_u^+;1_u,0_u^-)$ starts with this expression for the radiative transition rate from v' to all levels v'' of the ground-state dimer $Ar_2(^1\Sigma_g^+;0_g^+)$:

$$A_{v'}=\sum_{v''} A_{v';v''}+\int dE_{v''}\rho(E_{v''})A_{v',v''} . \tag{5.1a}$$

$A_{v',v''}$ is the radiative transition rate between vibrational level v' of $Ar_2^*(^3\Sigma_u^+;1_u,0_u^-)$ and vibrational level v'' of $Ar_2(^1\Sigma_g^+;0_g^+)$. All the v' levels are discrete; the summation in Eq. (5.1a) is over the discrete v'' levels of $Ar_2(^1\Sigma_g^+;0_g^+)$, while the integral is over the continuum v'' levels of the steeply repulsive van der Waals inner potential wall of $Ar_2(^1\Sigma_g^+;0_g^+)$. $\rho(E_{v''})$ is the continuum density of states (DOS) at energy $E_{v''}$ above the dissociative limit of $Ar_2(^1\Sigma_g^+;0_g^+)$.

Near the equilibrium internuclear separation of $Ar_2^*(^3\Sigma_u^+;1_u,0_u^-)$, the transition rate to the ground state is weak because it is spin forbidden. At larger internuclear separations, however, spin-orbit coupling causes the transition to become partially allowed. Consequently, $A_{v',v''}$ is calculated using the dipole approximation[27,28]

$$A_{v',v''}=(4/3c^3)(\Delta E)^3|\langle\phi_{v'}|\mu(R)|\phi_{v''}\rangle|^2 . \tag{5.1b}$$

Equation (5.1b) is in atomic units. c is the speed of light; $\Delta E=E_{v'}-E_{v''}$ is the radiative transition energy between $Ar_2^*(^3\Sigma_u^+;1_u,0_u^-)$ and $Ar_2(^1\Sigma_g^+;0_g^+)$; $\phi_{v'}$ and $\phi_{v''}$ are vibrational wave functions of the two respective electronic states; and $\mu(R)$ is the transition moment between the two electronic states as a function of internuclear separation R. For the electronic transition considered here, $\mu(R)$ has been calculated and tabulated.[27]

From Eqs. (5.1a) and (5.1b) it is noted that $A_{v'}$ for a given v' contains contributions from radiative transitions over a range of different transition energies ΔE. At transition energies for which the differential transition rate is relatively high, the spectrum will be relatively intense. Consequently, to obtain the luminescence spectrum $S_{v'}$ of level v', it is necessary to express Eq. (5.1a) differentially, in either energy or wavelength:

$$S_{v'}(\lambda)=dA_{v'}(\lambda)/d\lambda . \tag{5.2}$$

The wavelength is $\lambda=hc/\Delta E$, where h is Planck's constant.

To calculate vibrational wave functions, a sixth-order difference equation is used to integrate the radial Schrödinger equation.[29,30] For bound solutions, a predictor-corrector scheme is used to evaluate the vibrational energy eigenvalues.[29,30]

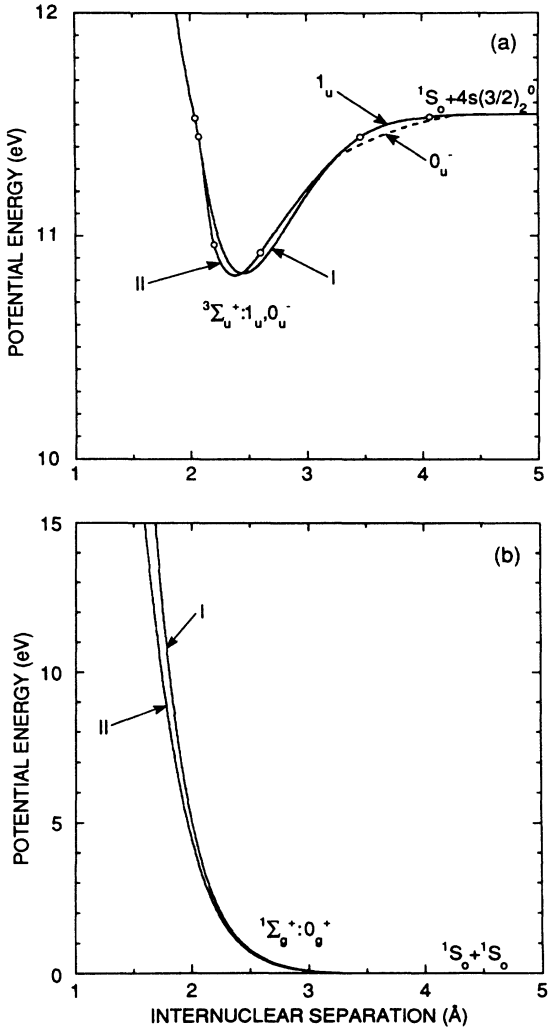

FIG. 13. Potential-energy surfaces used in the spectral simulations. (a) Comparison of excited-state Ar_2^* potential of Ref. 27 (I) and the excited-state potential used in this work (II). The spline points in (II) are indicated by open circles. An exaggerated schematic of the 0_u^- state is shown by the dashed line. (b) Comparison between available potential curves representing the van der Waals ground-state potential (the shallow wells, not visible on this scale, are identical between the two curves). Curve (I) is from Ref. 33, and curve (II) is from Ref. 34.

Potentials are chosen to represent the $Ar_2^*(^3\Sigma_u^+;1_u,0_u^-)$ and $Ar_2(^1\Sigma_g^+;0_g^+)$ electronic states. To represent $Ar_2^*(^3\Sigma_u^+;1_u,0_u^-)$, a potential published by Herman, LaRocque, and Stoicheff[31] is utilized. They have performed vuv laser spectroscopy on the levels $v'=24-30$. They have combined spectroscopic information about the top of the potential well with a theoretical calculation concerning the $v'=0$ level[32] and have tabulated a complete set of vibrational energy levels and potential surface turning points.[27] For $Ar_2(^1\Sigma_g^+;0_g^+)$, the empirical potential of Aziz and Slaman is used.[33] These two potential surfaces are shown in Figs. 13(a) and 13(b).

Calculated $A_{v'}$ based on these potentials agree quite well with the calculated results already published,[27] validating the computer program with which the present calculations are performed. Calculated radiative lifetimes for levels $v'=24-30$ agree very closely with excitation-state-selective time-resolved fluorescence decay measurements already published.[27] As v' decreases, the calculated lifetimes rise sharply for $v'<10$. However, the calculated lifetime for the $v'=0$ level, 8.5 μsec, greatly exceeds the experimental value, 3.0 μsec (Ref. 27 and references therein). This discrepancy is suggested to be due to an error in the extrapolation of the $Ar_2^*(^3\Sigma_u^+;1_u,0_u^-)$ potential to $v'=0$.[27] The $v'=0$ spectrum is calculated and shown in Fig. 14(a). It peaks at a wavelength of 1225 Å and displays a FWHM of 55 Å. As discussed next, this spectrum is too narrow and is positioned incorrectly in wavelength, and therefore the potentials used in the calculation are modified.

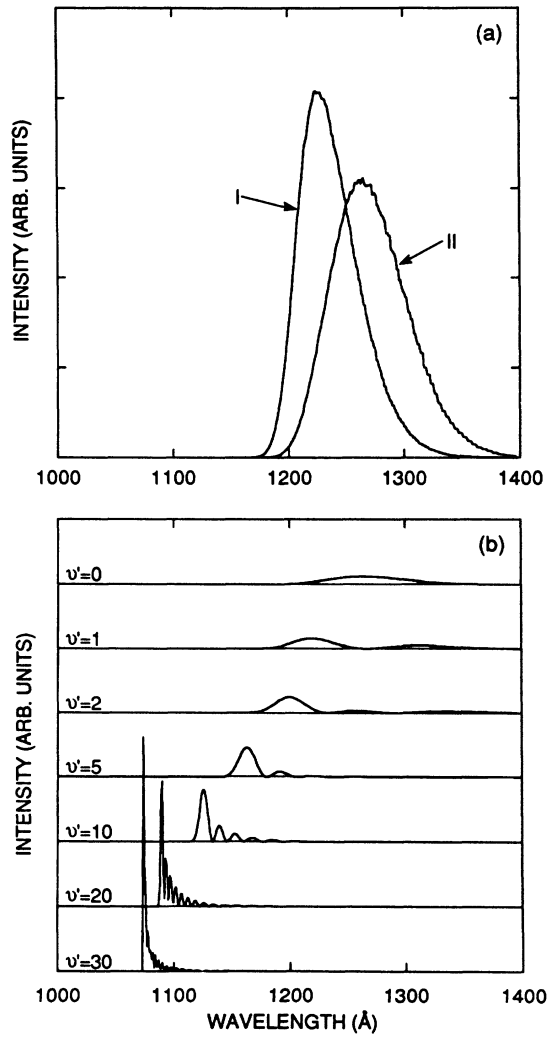

FIG. 14. Results of spectral simulations. (a) Computed $v'=0$ spectra based on potentials provided in Ref. 27 (curve I) and on modified potentials derived in the present work and discussed in Sec. V (curve II). (b) Simulated spectra for several different upper-electronic-state vibrational levels.

McLean, Liu, and Barker discuss a new potential to represent $Ar_2(^1\Sigma_g^+;0_g^+)$.[34] They claim that their *ab initio* calculation provides a better representation of the repulsive potential wall than does the potential of Aziz and Slaman,[33] but that the latter potential is an excellent representation of the bound portion of $Ar_2(^1\Sigma_g^+;0_g^+)$. McLean, Liu, and Barker offer a composite potential representing $Ar_2(^1\Sigma_g^+;0_g^+)$,[34] which is shown in Fig. 13(b).

A new potential to represent $Ar_2^*(^3\Sigma_u^+;1_u,0_u^-)$ is composed of three parts. The upper portion of the well, levels $v'=24-30$, is taken to be as given by Herman, LaRocque, and Stoicheff[31] because for those levels, the potential is based on rovibronic spectral analysis and is said to be accurate to within ± 0.05 Å. For $v'=0$, an offset Morse potential is used:

$$U(R)=E_0+D_e\{1-\exp[-a(R-R_e)]\}^2 . \quad (5.3)$$

The parameters a and D_e are related to the spectroscopic parameters ω_e and $\omega_e\chi_e$. A summary of the values of these parameters which have resulted from a number of experimental and theoretical studies performed on argon dimers appears in the literature.[35] A typical value of $\omega_e\chi_e$ is 2.8 cm^{-1}, from which $a=1.82$ $Å^{-1}$ is obtained. A typical value of ω_e is 290 cm^{-1}, from which $D_e=0.934$ eV is obtained. Finally, the equilibrium internuclear separation R_e and zero offset E_0 can be varied not only to result in a correct calculation of the $v'=0$ spectrum, but also to ensure that the $v'=24-30$ energy levels are still correctly calculated when the two potential pieces are splined together using a cubic spline.

A number of references contain information on the peak position and FWHM of the $v'=0$ spectrum for gas-phase excited argon. Both particle beams (ions,[36-38] electrons[39-41]) and plasma discharges[42-44] have been used to excite gas-phase argon. Owing to the high pressures employed in these types of experiments, it is expected that vibrational relaxation occurs very efficiently so that the observed emission spectrum is characteristic of fully relaxed $v'=0$ Ar_2^*. In spite of this expectation, however, particle beam excitation yields consistently narrower spectra than plasma discharges, the sole exception being in the case of excitation by relativistic electrons.[41] From the observations of the $v'=0$ spectrum in particle beam-excited gas-phase argon,[36-40] the peak wavelength can be taken to be 1265 Å, and the FWHM can be assumed to be in the range 70–80 Å. The $v'=0$ spectra of

$Ar_2^*(^3\Sigma_u^+;1_u,0_u^-)$ and $Ar_2^*(^1\Sigma_u^+;0_u^+)$, observed simultaneously in the gas-phase experiments, are expected to be displaced from each other by only about 5 Å, as observed from electronically excited solid-phase argon.[1]

The final potential representing $Ar_2^*(^3\Sigma_u^+;1_u,0_u^-)$ is shown in Fig. 13(a); the spline points are indicated. A very slight change in the model potentials makes a dramatic difference in the calculated $v'=0$ spectrum, shown in Fig. 14(a). The gross features of the calculated $v'=0$ spectrum are now in agreement with those of the observed $v'=0$ spectrum. Transition rates $A_{v'}$ are recalculated using the improved potentials. Calculated lifetimes for $v'=24-30$ agree well with observed ones, as before, but the calculated lifetime for $v'=0$ is now in poorer agreement with observations than before. This could reflect uncertainty in the transition moment data in the vicinity of R_e.[27] Since the object is to perform a spectral fit, the validity of the calculated lifetime for $v'=0$ has been sacrificed in favor of accuracy in the calculated $v'=0$ spectrum. Examples of calculated spectra are shown in Fig. 14(b).

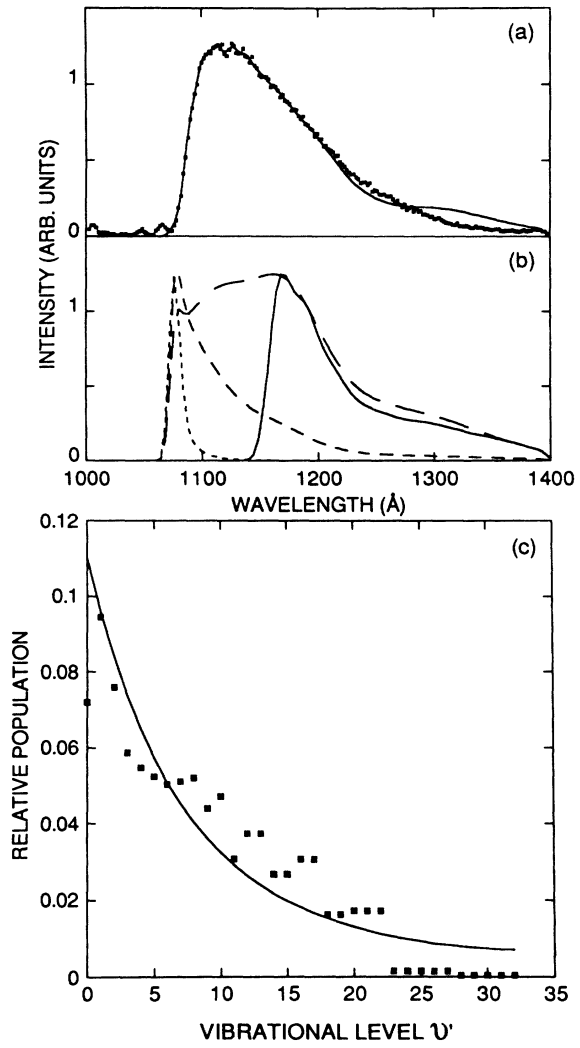

FIG. 15. Result of spectral fitting to the observed plume luminescence spectrum. (a) Dots represent the measured plume luminescence spectrum; the line is the result of a fit to a linear combination of the simulated spectra from upper-state vibrational levels v'. (b) Luminescence spectra obtained assuming various vibrational level population distributions. Small dashes: equal population in top six v' only, all other v' unoccupied. Long dashes: equal population in all v'. Solid line: equal population in bottom six v' only, all other v' unoccupied. Long dashes: Boltzmann population distribution characterized by $T=3000$ K. (c) Dots represent population distribution derived from the fit shown in (a). The solid line is the Boltzmann population distribution used in (b).

The luminescence spectrum of desorbed $Ar_2^*(^3\Sigma_u^+;1_u,0_u^-)$ is observed by orienting the target to a grazing angle of $\theta=49°$. This spectrum, displayed in Fig. 6, is approximately corrected for scattered M-band luminescence, grating reflectivity, and channelplate detection efficiency[45] and is then normalized to unit area. The simulated spectra $S_{v'}(\lambda)$ are each broadened to reflect the resolution used during the acquisition of the data. Each $S_{v'}(\lambda)$ is normalized to unit area. A general linear least-squares fit is then performed to express the observed spectrum as a linear combination of the $S_{v'}(\lambda)$. For high values of v', the simulated spectra are not sufficiently unlike one other to effect a unique fit; consequently, levels $v'=12$ and 13, $v'=14$ and 15, $v'=16$ and 17, $v'=18$ and 19, $v'=20-22$, $v'=23-27$, and $v'=28-32$ are, respectively, grouped together in subgroups within which the v' levels are assumed to have equal populations. The resulting fit and relative vibrational level occupancy distribution is shown in Figs. 15(a) and 15(c). It is immediately seen that the populations of the vibrational levels decline steeply with increasing vibrational quantum number v'. The ejected $Ar_2^*(^3\Sigma_u^+;1_u,0_u^-)$ are described as displaying a large degree of vibrational relaxation.

Based strictly on Poisson statistical variations in the spectral data, the fitted vibrational level occupancies are uncertain by about ±10%. However, the deviation of the fitted spectrum from the actual one for $\lambda>1210$ Å is obviously systematic and is not understood in detail. It is felt that this deviation is related to uncertainties in the model interaction potential for low-lying v' of $Ar_2^*(^3\Sigma_u^+;1_u,0_u^-)$, despite the care taken to simulate the $v'=0$ spectrum as accurately as possible.

Despite the systematic deviation of the fit from the data for $\lambda>1210$ Å, the qualitative trend of decreasing state occupancy with increasing vibrational quantum number v' of Ar_2^* is not affected by altering details of the fit. The same trend is observed even if the observed "raw" spectrum is used in the curve fit with no correction made for the channeltron photoelectron emission efficiency, the grating vuv reflectivity, or both. Also, the same general trend is obtained by fitting to $S_{v'}(\lambda)$ simulated using the potential surfaces employed by Herman, LaRocque, and Stoicheff[31] and by Madej and Stoicheff.[27]

Several spectra calculated assuming simple v'-level population distributions appear in Fig. 15(b). The only calculated spectrum displaying a width close to that of the observed spectrum results from an assumed Boltzmann distribution with a temperature of $T=3000$

K. However, no Boltzmann distribution results in a high-quality fit to the whole spectrum. From Fig. 15(c) it may be seen that low-v' and high-v' portions of the v'-level population distribution cannot simultaneously be fit to the same Boltzmann distribution. It is concluded that the v'-level population distribution of the desorbed Ar_2^* is non-Boltzmann.

VI. EVIDENCE FOR LUMINESCENCE FROM DESORBED METASTABLE $Ar_2^*(0_u^-)$

The luminescence time decays measured at wavelengths in the W band of desorbed Ar_2^*, shown in Fig. 8, all display a prominent long-lived "tail." The radiative lifetimes of $Ar_2^*(^3\Sigma_u^+;1_u,0_u^-)$ increase monotonically with degree of vibrational relaxation, ranging from 166 nsec for high v' to 3 μsec for $v'=0$.[27] Therefore, a maximum lifetime of 3 μsec should be observed in the luminescence time decays. However, when the lifetime of the tail of the 1100-Å decay is treated as a free fitting parameter, it is estimated to be 5.6 μsec, and this is considered a lower bound because the long-lived luminescence is not examined for a sufficiently long time to accurately identify an exact lifetime. Also, a luminescence time decay is calculated from the simulated spectra $S_{v'}(\lambda)$ and transition rates $A_{v'}$ for an observation wavelength of 1110-Å and a resolution of 25 Å and is also shown in Fig. 8. Although the quantum mechanical calculation of transition rates results in oversized lifetimes for most vibrational levels,[27] a result observable for $t<1$ μsec, there is no sign of a long-lived decay.

The spatial dependence of the plume luminescence, shown on a 1-cm scale in Fig. 7, also suggests the existence of luminescence characterized by a lifetime greater than 3 μsec. Assuming a hemispherical plume, the spatial dependence of the luminescence is modeled employing an ejection KE of around 0.1 eV and average lifetimes of 3 or 10 μsec. As shown in Fig. 7, assuming a lifetime of 3 μsec results in a model with much too short a spatial tail. To obtain a reasonable likeness to the data, considerably longer lifetimes must be assumed.

An understanding of long-lived luminescence observed at shorter wavelengths is derived from a consideration of the possible electronic states of Ar_2^*, discussed at length in Refs. 31 and 46. Relevant potential surfaces are shown in Fig. 13. The electronic states are labeled: $Ar_2^*(^3\Sigma_u^+;1_u,0_u^-)$, $Ar_2^*(^1\Sigma_u^+;0_u^+)$, and $Ar_2(^1\Sigma_g^+;0_g^+)$. Detailed analysis of vuv laser-induced fluorescence (LIF) measurements shows that the 1_u and 0_u^- states are degenerate for vibrational levels $v'<17$, leading to case (b) Hund's rule angular momentum coupling and to the state $^3\Sigma_u^+$. For the higher vibrational levels, the degeneracy is broken, and 0_u^- is slightly lower in energy than 1_u, but 1_u and 0_u^- again become degenerate in the separated atom limit.

Luminescence lifetimes of the states $Ar_2^*(1_u)$ and $Ar_2^*(^3\Sigma_u^+;1_u,0_u^-)$ are less than or equal to 3 μsec, as discussed earlier. By contrast, transitions from high v' levels of the metastable molecular state $Ar_2^*(0_u^-)$ to the ground-state $Ar_2(^1\Sigma_g^+;0_g^+)$ are said to be strongly forbidden. However, this is the only state which could possibly give rise to luminescence at wavelengths ranging from 1090 to 1150 Å and characterized by lifetimes greater than 3 μsec. LIF from the $Ar_2^*(0_u^-)$ state optically excited from gas-phase Ar_2 has not been observed,[31] but possibly only because the LIF is difficult to both excite and observe optically. In electronically excited *solid* argon, however, transitions that are forbidden radiatively are *allowed nonradiatively,*[47] and so for both ion and photon excitation of the allowed, higher-lying states of *solid* argon, optically forbidden states such as $Ar_2^*(0_u^-)$ could be formed and the species subsequently desorbed by some mechanism. It is thus hypothesized that the long spatial and temporal "tails" observed for $\lambda<1150$ Å are due to luminescence from desorbed metastable $Ar_2^*(0_u^-)$.

Based on Figs. 7 and 8, the fraction of the plume consisting of metastable luminescence is of the order of 10% of the total luminescence signal. Thus, even though the emission spectra of the $v'>17$ levels of the $Ar_2^*(0_u^-)$ state are unknown, failure to include them in the spectral fitting does not strongly influence the deduced vibrational level population distributions derived above.

VII. DISCUSSION

The KE and state of vibrational relaxation of desorbed Ar_2^* are important clues to the desorption process. The typical KE of desorbed Ar_2^* is 0.1 eV; the spread in KE is large and the maximum KE is 0.3 eV. Ar_2^* are desorbed in a wide range of degree of vibrational relaxation, but the population distribution is peaked at $v'=0$ and 1. Desorbed Ar_2^* that are more relaxed vibrationally display slightly higher KE than desorbed dimers that are less relaxed vibrationally; internal energy is anticorrelated with the center-of-mass (cm) KE.

One model describing the ejection of excited species from solid argon is the cavity ejection model.[6,10–13,15,16,20,48] Solid argon is characterized by a negative electron affinity.[49] The Rydberg electron associated with an excited center such as Ar^* or Ar_2^* thus causes lattice distortion in the form of a cavity around the excited center. Cavities exist around ASTE's and MSTE's in bulk argon, as shown schematically in Figs. 1(a) and 1(g). If the excited species is located on the surface of the Ar film, the formation of a cavity may cause the excited species to be ejected. This process is shown for Ar^* and Ar_2^* in Figs. 1(c) and 1(e). Molecular dynamics calculations have been performed to see if cavity ejection is feasible.[20,48] The results of these calculations for Ar_2^* (Ref. 20) and Ar^* (Ref. 48) are shown in Table I. Unrelaxed $Ar_2^*(^3\Sigma_u^+;1_u,0_u^-)$ on the surface eject in less than 1 psec, well before vibrational relaxation can take place. The calculated KE is very low, 0.02 eV. Excited species located at "damaged" sites on the surface are ejected with even lower KE, if they are even ejected at all. Under excitation of Ar films by electrons and vuv photons, ejected metastable Ar^* have been detected with KE of the order of 0.04 eV,[10,11] consistent with the calculated KE for cavity-ejected Ar^*. However, cavity ejection does not account for the major fraction of ejected Ar_2^* observed under 1.5-MeV He^+-ion excitation.

TABLE I. Kinetic energies of cavity-ejected atoms and dimers from classical dynamics simulations of electronically excited solid argon.

Crystal face	Atoms[a]	Vibrationally excited dimers[b]
(100)	0.024 eV	0.02 eV
(111)	0.055 eV	0.02 eV

[a]Reference 52.
[b]Reference 53.

Under 1.5-MeV He^+-ion excitation of solid argon, the dominant excitation mechanism is the creation of electron-hole pairs. Energetic ejection of Ar_2^* may arise as a consequence of repulsive recombination of self-trapped holes, as summarized in Figs. 1(d) and 2. Electron recombination with a self-trapped hole[5,6,8] Ar_2^+, or repulsive predissociation of a highly electronically excited dimer Ar_2^{**}, results in an energetic repulsive separation of a ground-state Ar and an excited state Ar* (process 2 in Fig. 2). The moving Ar* atom could dimerize near the surface in a multibody collision, disposing of variable amounts of excess vibrational energy. There could easily be enough energy left over for the resulting Ar_2^* to be ejected with considerable KE. The anticorrelation between internal vibrational energy and the cm KE is indicative of a final collisional process that channels vibrational energy into KE of motion. Molecular dynamics calculations are in progress to examine the validity of this desorption mechanism and preliminary results demonstrate its viability.[16,22]

Experimental evidence supporting the existence of repulsive recombination events has been obtained by Arakawa, Takahashi, and Takeuchi[10] and Arakawa and Sakurai[11] in their investigation of photon-stimulated desorption of metastable Ar*. If only the lowest-energy excitonic state of an argon film is excited by vuv synchrotron radiation, repulsive recombination and predissociative decays are energetically *impossible,* and ejection only of *low*-KE (0.04 eV) Ar* is observed. This low KE is consistent with the cavity ejection mechanism shown in Fig. 1(e).[10,11,13,48] If the vuv photons are tuned to excite excitons for which repulsive predissociation *is possible,* then additional Ar* are observed with a *much higher* KE around 0.5 eV. These high-KE ejected atoms are the result of repulsive predissociation events for which Ar* is able to escape the surface without forming Ar_2^*. A similar process, labeled 2 in Fig. 2 and shown in Fig. 1(f), would occur after repulsive recombination of the self-trapped hole Ar_2^+.

In the gas phase, linearly bonded ionic trimers Ar_3^+ are slightly more stable than the ionic dimer Ar_2^+.[50] Consequently, electron recombination processes at ionic trimer sites may play an important role in the desorption process. A detailed consideration of possible desorption mechanisms associated with ionic trimer sites is beyond the scope of this paper. However, two general scenarios for such desorption mechanisms can be suggested. First, upon electron recombination of an electron with Ar_3^+, the complex Ar_2^*-Ar could form. Then the same force that normally gives rise to cavity formation around Ar_2^* could cause the Ar_2^* and Ar of the neutral trimer complex to separate with some yield of KE. Although the force that gives rise to cavity formation is "gentle," in the case of Ar_2^*-Ar a ground-state Ar is closer to the Ar_2^* than is the case for an Ar_2^* interacting equally with a number of ground-state nearest neighbors, and therefore the force driving apart Ar_2^*-Ar may be quite strong. If the trimer repulsive recombination event occurs on the surface of the argon solid, the Ar_2^* may be ejected. Depending on the intersections between, and the dynamical behavior of atoms on the complex potential surfaces representing the interaction of three Ar atoms in various states, it could turn out that KE and potential energy (PE) of the desorbed Ar_2^* are anticorrelated. The second scenario is that upon electron recombination, Ar_3^+ could dissociate into three repulsively interacting atoms, Ar, Ar, and Ar*. If the Ar* happens to interact with at least two other Ar atoms near the surface, it could be desorbed as a dimer Ar_2^* as discussed above. In view of these two scenarios, it is expected that the repulsive recombination ejection mechanism will retain its general validity for both dimer Ar_2^+ and trimer Ar_3^+ precursor states as well as for higher-order ionic clusters in the solid.[51]

VIII. CONCLUSIONS

It has been shown that long-lived *W*-band luminescence comes dominantly from desorbed $Ar_2^*(^3\Sigma_u^+;1_u,0_u^-)$. The KE of desorbed $Ar_2^*(^3\Sigma_u^+;1_u,0_u^-)$ has been determined to be around 0.1 eV and ranges up to 0.3 eV. Spectral simulations and fitting to the observed spectrum indicate that the $Ar_2^*(^3\Sigma_u^+;1_u,0_u^-)$ are predominantly relaxed vibrationally during the ejection process. The observed KE is too high to be accounted for by the cavity ejection mechanism,[13,20] which also does not account for the observed degree of vibrational relaxation. Ejection due to repulsive electron-hole recombination[5,6] is expected to result in much larger KE's and in a much greater degree of vibrational relaxation. Preliminary classical dynamics simulations indicate the feasibility of this mechanism.[22]

The spatial plume distribution and the time dependence of the plume luminescence show evidence of a long-lived electronic state. It is hypothesized that this contribution is due to desorbed metastable $Ar_2^*(0_u^-)$. Luminescence from this state has not been previously identified.

ACKNOWLEDGMENTS

The work at the University of Virginia was supported by NSF Grant Nos. DMR-86-00469 and CBT-86-13614. This work was done while one of us (C.T.R.) was at the Naval Research Laboratory with partial support from the National Research Council. One of us (C.T.R.) thanks R. D. Carson for advice on data analysis programs, R. E. Johnson for helpful comments, and G. Dujardin for a useful discussion concerning the possible role played by Ar_3^+ in the dimer-desorption process.

*Present address: Department of Radiation Sciences, Uppsala University, Uppsala, Sweden.
†Present address: Department of Materials Science and Engineering, University of Pennsylvania, Philadelphia, PA 19104.

[1]N. Schwentner, E.-E. Koch, and J. Jortner, *Electronic Excitations in Condensed Rare Gases* (Springer-Verlag, Berlin, 1985), p. 126.
[2]F. Besenbacher *et al.*, Nucl. Instrum. Methods **191**, 221 (1981).
[3]O. Ellegaard *et al.*, Appl. Phys. A **46**, 305 (1988).
[4]J. Schou *et al.*, Nucl. Instrum. Methods Phys. Res. B **18**, 609 (1987).
[5]C. T. Reimann, R. E. Johnson, and W. L. Brown, Phys. Rev. Lett. **53**, 600 (1984).
[6]C. T. Reimann, W. L. Brown, and R. E. Johnson, Phys. Rev. B **37**, 1455 (1988).
[7]E. R. Moog, J. Unguris, and M. B. Webb, Surf. Sci. **134**, 849 (1983).
[8]D. J. O'Shaughnessy *et al.*, Phys. Rev. Lett. **61**, 1635 (1988).
[9]P. Feulner *et al.*, Phys. Rev. Lett. **59**, 791 (1987).
[10]I. Arakawa, M. Takahashi, and K. Takeuchi, J. Vac. Sci. Technol. A **7**, 2090 (1989).
[11]I. Arakawa and M. Sakurai, in *Desorption Induced by Electronic Transitions, DIET IV,* edited by G. Betz and P. Varga (Springer-Verlag, Berlin, 1990), p. 246.
[12]T. Kloiber and G. Zimmerer, Radiat. Eff. Def. Solids **109**, 219 (1989).
[13]F. Coletti, J. M. Debever, and G. Zimmerer, J. Phys. (Paris) Lett. **45**, L467 (1984).
[14]T. Kloiber, dissertation, Universität Hamburg, 1989 (unpublished).
[15]C. T. Reimann *et al.*, in *Desorption Induced by Electronic Transitions, DIET IV* (Ref. 11), p. 246.
[16]C. T. Reimann *et al.*, Nucl. Instrum. Methods Phys. Res. B **58**, 404 (1991).
[17]I. Ya. Fugol', Adv. Phys. **37**, 1 (1988).
[18]A. Hourmatallah, F. Coletti, and J. M. Debever, J. Phys. C **21**, 1307 (1988).
[19]E. Roick *et al.*, J. Phys. C **17**, 945 (1984).
[20]S.-T. Cui *et al.*, Phys. Rev. B **39**, 12 345 (1989).
[21]R. E. Johnson and M. Inokuti, Nucl. Instrum. Methods **206**, 289 (1983).
[22]D. E. Grosjean and R. E. Johnson (unpublished).
[23]*Rare Gas Solids,* edited by M. L. Klein and J. A. Venables (Academic, New York, 1977), Vols. I and II.
[24]S. I. Kovalenko and N. N. Bagrov, Fiz. Tverd. Tela (Leningrad) **11**, 2724 (1979) [Sov. Phys. Solid State **11**, 2207 (1970)].
[25]W. L. Weise, M. W. Smith, and B. M. Miles, *Atomic Transition Probabilities,* Natl. Stand. Ref. Data Ser., Nat. Bur. Stand. (U.S.) No. 22, (U.S. GPO, Washington, D.C., 1969), p. 192.
[26]A. A. Madej, P. R. Herman, and B. P. Stoicheff, Phys. Rev. Lett. **57**, 1574 (1986).
[27]A. A. Madej and B. P. Stoicheff, Phys. Rev. A **38**, 3456 (1988).
[28]B. Schneider and J. S. Cohen, J. Chem. Phys. **61**, 3240 (1974).
[29]J. W. Cooley, Math. Computation **XV**, 363 (1961).
[30]J. K. Cashion, J. Chem. Phys. **39**, 1872 (1963).
[31]P. R. Herman, P. E. LaRocque, and B. P. Stoicheff, J. Chem. Phys. **89**, 4535 (1988).
[32]J. H. Yates *et al.*, J. Chem. Phys. **79**, 6145 (1983).
[33]R. A. Aziz and M. J. Slaman, Mol. Phys. **58**, 679 (1986).
[34]A. D. McLean, B. Liu, and J. A. Barker, J. Chem. Phys. **89**, 6339 (1988).
[35]D. C. Shannon and J. G. Eden, J. Chem. Phys. **89**, 6644 (1988).
[36]O. Cheshnovsky, B. Raz, and J. Jortner, Chem. Phys. Lett. **15**, 475 (1972).
[37]O. Cheshnovsky, B. Raz, and J. Jortner, J. Chem. Phys. **59**, 3301 (1973).
[38]P. Millet *et al.*, J. Phys. B **15**, 2935 (1982).
[39]N. Thonnard and G. S. Hurst, Phys. Rev. A **5**, 1110 (1972).
[40]J. W. Keto, R. E. Gleason, Jr., and G. K. Walters, Phys. Rev. Lett. **33**, 1365 (1974).
[41]H. A. Koehler *et al.*, Phys. Rev. A **9**, 768 (1974).
[42]A. Gedanken *et al.*, J. Chem. Phys. **57**, 3456 (1972).
[43]R. C. Michaelson and A. L. Smith, J. Chem. Phys. **61**, 2566 (1974).
[44]Y. Tanaka, W. C. Walker, and K. Yoshino, J. Chem. Phys. **70**, 380 (1979).
[45]Information provided by Gallileo Corp. and Acton Research Corp.
[46]P. R. Herman, A. A. Madej, and B. P. Stoicheff, Chem. Phys. Lett. **134**, 209 (1987).
[47]G. Herzberg, *Spectra of Diatomic Molecules* (Van Nostrand Reinhold, New York, 1950).
[48]S.-T. Cui, R. E. Johnson, and P. T. Cummings, Phys. Rev. B **39**, 9580 (1989).
[49]J. Jortner et al., J. Chem. Phys. **42**, 750 (1965).
[50]W. R. Wadt, Appl. Phys. Lett. **38**, 1030 (1981).
[51]F. Carnovale, J. B. Peel, R. G. Rothwell, and P. J. Kunz, J. Chem. Phys. **90**, 1452 (1989).
[52]S.-T. Cui *et al.*, Phys. Rev. B **39**, 12 345 (1989).
[53]S.-T. Cui, R. E. Johnson, and P. T. Cummings, Phys. Rev. B **39**, 9580 (1989).

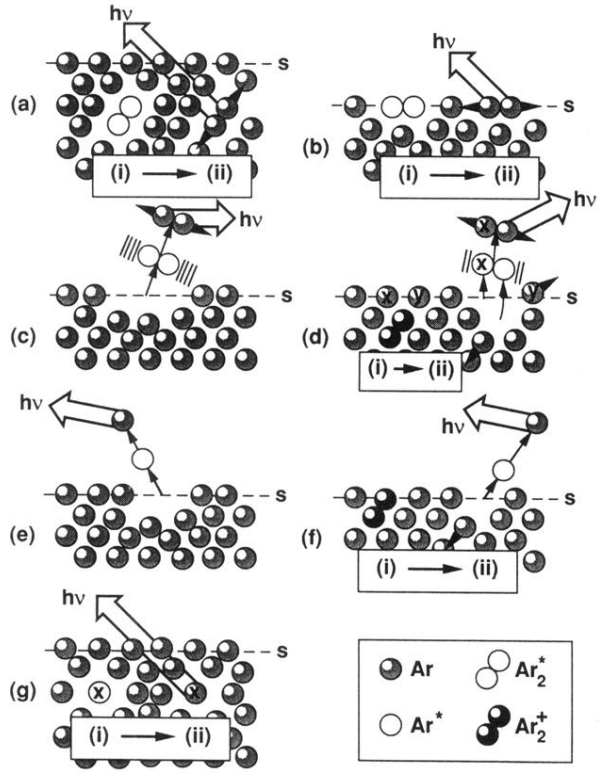

FIG. 1. Schematic of exciton and hole decay processes in solid argon. The steps in a given process proceed from (i) to (ii). (a) Cavity formation around a bulk self-trapped Ar_2^* and subsequent repulsive radiative decay; (b) surface self-trapped Ar_2^* and subsequent repulsive radiative decay; (c) cavity ejection of a vibrationally excited surface self-trapped Ar_2^* and subsequent radiative decay of the Ar_2^* in space; (d) repulsive recombination of an electron with Ar_2^+ and subsequent ejection of vibrationally excited Ar_2^* (electron not shown). The energized atom moving towards the surface has dimerized with the atom labeled "*x*." During dimerization, vibrational relaxation occurs through a collision with atom "*y*" and some other nearby surface atoms. Radiative decay occurs in space; (e) cavity ejection of a surface self-trapped Ar^* and eventual radiative decay in space; (f) repulsive recombination of an electron with Ar_2^+ and subsequent ejection of Ar^* (electron not shown) and eventual radiative decay in space; (g) cavity formation around a bulk self-trapped Ar^* and subsequent radiative decay.